2020 IEEE/RSJ International Conference on Intelligent Robots and Systems (IROS)
October 25-29, 2020, Las Vegas, NV, USA (Virtual)

Toward Analytical Modeling and Evaluation of Curvature-Dependent Distributed Friction Force in Tendon-Driven Continuum Manipulators

Yang Liu[1], Seong Hyo Ahn[1], Uksang Yoo[1], Alexander R. Cohen[1], and Farshid Alambeigi[1]

***Abstract*— In this paper, we present an analytical modeling approach to address the problem of tension loss in a generic variable curvature tendon-driven continuum manipulators (TD-CM) occurring due to the tendon-sheath distributed friction force. Despite the previous approaches in the literature, our presented model and the iterative solution algorithm do not rely on *a priori* known curvature/shape of the TD-CM and can be implemented on any TD-CM with constant/ variable curvatures with a continuous neutral axis function. The performance of the proposed modeling approach in predicting the distributed tendon tension and tension loss has been evaluated via simulation and experimental studies on a TD-CM with planar bending. Results demonstrate the outstanding and accurate performance of our novel modeling and the proposed solution algorithm.**

I. Introduction

Tendon-Driven Continuum Manipulators (TD-CMs) have gained increasing popularity in various minimally invasive single-port, multi-port, and natural orifice surgical robotic applications [1]. For instance, various types of TD-CMs have been utilized for minimally invasive treatment of orthopedic applications [2], [3], single-incision laparoscopic [4]. This is mainly due to the excellent features of a tendon-driven actuation mechanism that enable safe and remote transmission of power to the robot's end-effector using a lightweight and miniaturized tendon-sheath mechanism [1], [5]. However, the adverse effects of tendon-sheath friction along the transmission line (typically, the body of CM as shown in Fig. 1) may result in significant non-uniform tendon tension and subsequently tension/motion losses [5], [6]. These considerable losses affect the deformation behavior of a TD-CM, which need to be considered during the modeling and design phases before fabrication of the robot. Additionally, appropriate TD-CM deformation behavior modeling considering the tendon-sheath friction can mitigate challenges associated with the CM's accurate control, shape sensing, and contact detection with the environment [1].

A review of literature demonstrates the efforts of researchers in modeling the deformation behavior of TD-CMs using different approaches while mainly ignoring the effect of tendon-sheath friction. For instance, piece-wise constant curvature approaches have been utilized in different studies (e.g., [7], [8]), which work based on the imperfect assumption that the curvature of a small section in the CM is constant along its arc length [9]. Additionally, geometrically exact models, mainly based on Cosserat rod theory, have also been adapted for modeling various types of Variable Curvature (VC) TD-CMs (e.g., [10]). Till et al. [9] has recently reviewed Cosserat-rod-theory-based modeling approaches for different types of CMs.

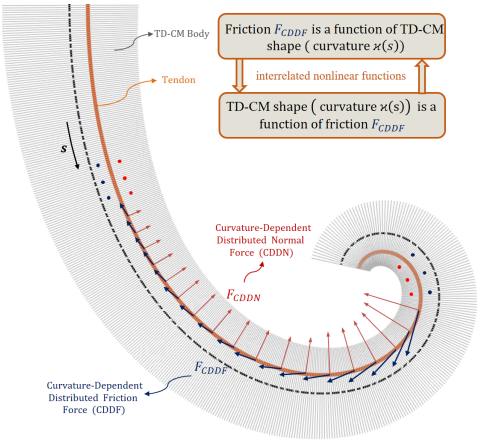

Fig. 1. Conceptual illustration of the curvature-dependent distributed friction/normal force in TD-CMs and its interrelated relation with curvature.

On the other hand, various approaches have been suggested by researchers to consider the effect of friction in modeling the deformation behavior of CMs. For instance, Gao et al. [11] considered a simple point-load Coulomb friction model between the tendon and sheath of the TD-CM using Cosserat rod theory deformation modeling approaches. However, this simplified approach cannot accurately model the distributed friction force along the tendon-sheath transmission line. In [12], a modified Dahl friction formulation and lumped-mass model were utilized to model internal friction of a cardiac catheter. However, this model requires experimental data to determine the Dahl friction model parameters and it cannot be extended to a generic model used for other forms of CMs. Subramani et al. [13] proposed a nonlinear friction model to predict tension distribution of a catheter system based on linear elastic bending mechanics of CM. The least squares fitting techniques and experimental data were used to optimize the friction parameter. It is an optimization-based method and relies on experimental data. More recently, to estimate internal friction parameters for a VC-CM, a framework has been suggested by Roy et al. [6]. This approach is also optimization-based, and it requires experimentally-measured data to identify the friction parameters. Overall, review of the literature demonstrates that most of the current approaches have been mainly developed based on either simplifying assumptions (e.g., constant-

[1]Y. Liu, S. Ahn, U. Yoo, A. Cohen, and F. Alambeigi are with the Walker Department of Mechanical Engineering at the University of Texas at Austin, Austin, TX, 78712, USA. (Email: {liu.yang,ahnseonghyo,uy95, alexander.cohen}@utexas.edu, farshid.alambeigi @austin.utexas.edu).

curvature deformation behavior or point load friction forces) or optimization-based approaches that are not extendable to a generic analytical model of a VC-CM.

To address the aforementioned limitations and with the goal of introducing a generic approach for modeling the deformation behavior of a VC-CM, in this study, we extend the typical geometrically exact model based on the Cosserat rod theory and include the effect of Curvature-Dependent Distributed Friction (CDDF) Force between the tendon and sheath. Of note, in our derivation, we do not consider assumptions such as *a priori* known curvature/shape and/or constant-curvature deformation behavior for the TD-CM. For this study, we will focus on analytical modeling of the distributed friction force and tension loss along a generic TD-CM with a 2D planar bending and propose an iterative algorithm to calculate interrelated shape/curvature and CDDF force of a generic TD-CM. We also experimentally evaluate our derived analytical model and the proposed algorithm for solving this model on a fabricated TD-CM.

II. Problem Formulation

A. Problem Statement

Let's consider a *generic variable curvature TD-CM*, shown in Fig. 2, with an *unknown planar* deformation behavior. The goal of this paper is to derive a mathematical model to establish an analytical relation between the known actuation input (i.e., tendon tension(s) at the base of the CM, T_{base}), and unknown deformation behavior of a VC-CM, while considering the effect of a curvature-dependent distributed friction force on the tendon(s) tension loss along the TD-CM. With this objective in mind, we make the following assumptions/remarks:

Remark 1: It is worthwhile to emphasize that, CDDF force and shape/curvature in a TD-CM are interrelated, which makes their mathematical modeling very complex. To mitigate this modeling problem, most of the literature (e.g.,[12], [13]) either considered *a priori* known shape/curvature for the CM to calculate the friction force or completely ignored the tendon friction to model the shape of a TD-CM. However, in this paper, we assume these parameters (i.e., the CDDF force and shape of the CM) both are unknown and entangled and completely consider the effect of tendon-sheath friction on deformation behavior of a generic TD-CM and vice versa.

Remark 2: Although, in this paper, we have considered a conical geometry for our modeled VC-CM, the proposed modeling approach is generic and can be applied on any CM with different geometry in which the neutral axis is a smooth differentiable function of arc length s.

Remark 3: From now on and for the sake of simplicity throughout the paper, we use the acronym "VC-CM" to refer to a "variable curvature tendon-driven continuum manipulator".

B. Considered Reference Frames

As shown in Fig. 2, to model deformation behavior of a generic conical-shaped VC-CM, we first define a fixed frame $\{X-Y\}$ located at the base of the manipulator and use local

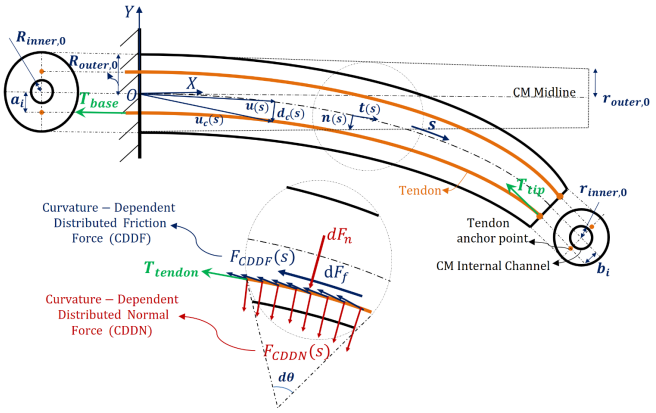

Fig. 2. Conceptual illustration of a generic VC-CM with planar bending.

2D Frenet–Serret reference frames $(\vec{t}(s), \vec{n}(s))$ to describe the position and orientation of arbitrary cross sections along the VC-CM midline. The following describes the equations relating these two reference frames:

$$\begin{cases} \dfrac{d\vec{t}}{ds} = \kappa(s)\vec{n}(s) \\ \dfrac{d\vec{n}}{ds} = -\kappa(s)\vec{t}(s) \\ \dfrac{d\vec{u}}{ds} = \vec{t}(s) \end{cases} \tag{1}$$

where s represents the arc length parameter along the VC-CM midline, $\kappa(s)$ represents the curvature of the midline (neutral axis) as a function of s, and $\vec{t}(s)$ and $\vec{n}(s)$ are the tangential and normal vectors to the midline curve, respectively. Also, $\vec{u(s)}$ describes the position of the origin of these local frames with respect to the fixed frame $\{X-Y\}$.

Using these frames, we can also continuously define the position $\vec{u_{\text{ci}}}(s)$ of the i^{th} tendon $i = \{1, 2\}$ passing through a conical sheath (or CM's body, as shown in Fig. 2) based on the arc length parameter s as follows:

$$\begin{cases} \vec{u_{\text{ci}}}(s) = \vec{u}(s) \pm d_{\text{ci}}\vec{n}(s) \\ d_{\text{ci}}(s) = a_i - \dfrac{s\,(a_i - b_i)}{L} \end{cases} \tag{2}$$

where a_i and b_i are the distances between the tendons locations to the midline at the base and tip cross sections of the VC-CM, respectively (Fig. 2). Also, $d_{\text{ci}}(s)$ is a function defining the distance between the tendons' location and the midline and L is the overall length of the VC-CM.

Using (1) and (2), we can derive the tangential unit vector for each tendon $\vec{t_{ci}}(s)$ as well as the curvature along each tendon κ_{ci} using the following equations:

$$\vec{t_{ci}}(s) = \frac{d\vec{u_{ci}}}{ds}, \kappa_{\text{ci}}(s) = \frac{1}{\dfrac{1}{\kappa(s)} \pm d_{\text{ci}}(s)} \tag{3}$$

where here we assume the tendon arc length s_c can be approximated by the midline arc length s.

C. Modelling Curvature-Dependent Distributed Friction Force in a Generic VC-CM

As shown in Fig. 2, relations among the normal force F_n, friction force F_f, and tendon tension T_{tendon} in a differen-

tial element along the tendon-sheath of a VC-CM can be described using the following equations [13], [5]:

$$\begin{cases} dT_{\text{tendon}} = dF_f \\ dF_f = \mu dF_n = \mu \mathrm{T}_{\text{tendon}} d\theta \end{cases} \tag{4}$$

where μ is the friction coefficient of the relative motion between the tendon and sheath/manipulator body and $d\theta$ is the differential tendon wrap/bending angle of the VC-CM.

Considering (4), we can describe the relation between the tendon tension at the base T_{base} and tip T_{tip} of a VC-CM based on the overall tendon wrap/bending angle θ along the tendon length as follows:

$$\begin{cases} \dfrac{dT_{\text{tendon}}}{T_{\text{tendon}}} = \mu d\theta \\ \displaystyle\int_{T_{\text{tip}}}^{T_{\text{base}}} \frac{1}{T_{\text{tendon}}}\, dT_{\text{tendon}} = \mu\theta \\ \ln\left(T_{\text{base}}\right) - \ln\left(T_{\text{tip}}\right) = \ln\left(\dfrac{T_{\text{base}}}{T_{\text{tip}}}\right) = \mu\theta \end{cases} \tag{5}$$

Additionally, wrap/bending angle $\theta_i(s)$ of the i^{th} tendon can be related to the curvature κ_{ci} over the arc length of the tendon , as shown in (6). Using (3), (5), and (6), we can now obtain (7) to calculate $\vec{T}_{\text{tip}}$, the vector of tendon tension at the tip of a VC-CM.

$$\theta_i(s) = \int_0^s \kappa_{ci}(\xi)\, d\xi \tag{6}$$

$$\vec{T}_{\text{tip,i}} = -T_{\text{base,i}}\vec{t}_{ci}(L)e^{-\mu\theta_i(L)} = -T_{\text{base,i}}\vec{t}_{ci}(L)e^{-\mu\int_0^L \kappa_{ci}(\xi)\, d\xi} \tag{7}$$

More generally, we can use (3), (5), and (6) to calculate the vector of tendon tension at any arbitrary point $\vec{T}_{tendon}(s)$ based on a variable curvature along the tendon arc length $\kappa_{ci}(s)$:

$$\vec{T}_{\text{tendon,i}}(s) = -T_{\text{base,i}}\vec{t}_{ci}(s)e^{-\mu\int_0^s \kappa_{ci}(\xi)\, d\xi} \tag{8}$$

Using (1-4) and (8), at any arbitrary point along the arc length s, we can calculate the Curvature-Dependent Distributed Normal (CDDN) force $F_{\text{CDDN}}(s)$ and the CDDF force $F_{\text{CDDF}}(s)$ of a generic VC-CM as the following:

$$\vec{F}_{\text{CDDN,i}}(s) = T_{\text{tendon,i}}(s)\frac{d\vec{t_{ci}}(s)}{ds} = T_{\text{base,i}}\frac{d\vec{t_{ci}}(s)}{ds}e^{-\mu\int_0^s \kappa_{ci}(\xi)\, d\xi} \tag{9}$$

$$\begin{aligned} \vec{F}_{\text{CDDF,i}}(s) &= -\mu F_{\text{CDDN,i}}(s)\vec{t_{ci}}(s) \\ &= -T_{\text{base,i}}\mu\kappa_{ci}(s)\frac{d\vec{u_{ci}}(s)}{ds}\cdot e^{-\mu\int_0^s \kappa_{ci}(\xi)\, d\xi} \end{aligned} \tag{10}$$

Of note, (8), (9), and (10) describe the distributed tendon tension, distributed normal force, and distributed friction force along tendon(s) of a generic VC-CM, respectively, and have been derived without considering any assumptions. These forces are used in the next section to obtain the deformation behavior/shape of a VC-CM.

D. Modeling the Deformation Behavior of a Generic VC-CM Based on the CDDF Force

To obtain the deformation behavior (i.e., shape/curvature) of a generic VC-CM, in this section, we use the Euler-Bernoulli beam theory and the derived forces in Section II-C to relate the actuation input (i.e., tendon tension(s)) to the to the configuration variable (i.e., curvature of the VC-CM $\kappa(s)$) along its neutral axis as follows:

$$EJ(s)\kappa(s) = M(s) \tag{11}$$

where E is the Young's modulus of the VC-CM and $J(s)$ is the second moment of area of the VC-CM's cross section along its arc length.

For a generic conical-shaped VC-CM with an internal channel (as shown in Fig. 2), the second moment of area about the neutral axis can be represented by a smooth and differentiable function as the following:

$$\begin{cases} J(s) = \dfrac{\pi}{4}(R_{\text{outer}}(s)^4 - r_{\text{inner}}(s)^4) \\ R_{\text{outer}}(s) = R_{\text{outer,0}} - \dfrac{s\left(R_{\text{outer,0}} - r_{\text{outer,0}}\right)}{L} \\ r_{\text{inner}}(s) = R_{\text{inner,0}} - \dfrac{s\left(R_{\text{inner,0}} - r_{\text{inner,0}}\right)}{L} \end{cases} \tag{12}$$

where $R_{outer,0}$ and $R_{inner,0}$ describe the outer and inner radii of the VC-CM circular cross section at its base, while $r_{outer,0}$ and $r_{inner,0}$ represent the outer and inner radii of the VC-CM circular cross section at its tip, respectively. Also, $R_{outer}(s)$ and $R_{inner}(s)$ are the outer and inner radii of the circular cross section of the VC-CM at an arbitrary point s.

To use (11), we first need to calculate the total moment at each cross section due to the point load T_{tip} at the tip of the VC-CM (obtained by (7)) as well as the CDDN and CDDF forces (obtained by (9) and (II-C), respectively) along the VC-CM as the following:

$$\begin{aligned} \vec{M}_i(s) = \int_s^L T_{\text{base,i}}e^{-\mu\int_0^s \kappa_{ci}(\xi)\, d\xi}\left(\frac{d\vec{t}_{ci}(\xi)}{d\xi} - \right. \\ \left.\mu\kappa_{ci}(\xi)\frac{d\vec{u}_{ci}(\xi)}{d\xi}\right) \times \left(\vec{u}(s) - \vec{u}_{ci}(\xi)\right)\, d\xi - T_{\text{base,i}}\vec{t}_{ci}(L)\cdot \\ e^{-\mu\int_0^L \kappa_{ci}(s)\, ds} \times \left(\vec{u}(s) - \vec{u}_{ci}(L)\right) \end{aligned} \tag{13}$$

where $(...)\times(...)$ denotes the cross product of an appropriate force vector and moment arm, respectively.

Substituting (12) and (13) in the Euler-Bernoulli equation (11), we can now obtain the following static equation relating the distributed tendon tension, friction, and normal forces to the shape of a generic VC-CM described by its neutral axis curvature $\kappa(s)$:

$$\begin{aligned} EJ(s)\kappa(s) = \sum_{i=1}^{2}[\int_s^L T_{\text{base,i}}e^{-\mu\int_0^s \kappa_{ci}(\xi)\, d\xi}\left(\frac{d\vec{t}_{ci}(\xi)}{d\xi} - \right. \\ \left.\mu\kappa_{ci}(\xi)\frac{d\vec{u}_{ci}(\xi)}{d\xi}\right) \times \left(\vec{u}(s) - \vec{u}_{ci}(\xi)\right)\, d\xi - T_{\text{base,i}}\vec{t}_{ci}(L)\cdot \\ e^{-\mu\int_0^L \kappa_{ci}(s)\, ds} \times \left(\vec{u}(s) - \vec{u}_{ci}(L)\right)] \end{aligned} \tag{14}$$

III. Proposed Iterative Algorithm to Solve the VC-CM Deformation Behavior Model

As mentioned in Remark 1 and can be understood from (14), deformation behavior/shape of a VC-CM– which is described by its curvature– is the function of the distributed tendon(s) tension while the distributed tendon(s) tension itself is determined by the manipulator's shape. In other words, to solve this interrelated equation, one of the shape or distributed tension parameters needs to be known *a priori*.

To solve this problem without a priori knowledge on the shape or distributed tendon(s) tension, we propose an iterative algorithm comprising of the following two steps:

1) Step 1: Solving (14) when $F_{CDDF} = 0$: We first assume there is no tension loss due to the tendon-sheath friction force (i.e., $F_{\text{CDDF}} = 0$ and $T_{\text{base}} = T_{\text{tip}}$) and, therefore, simplify (14) as follows:

$$EJ(s)\kappa(s) = \sum_{i=1}^{2}[\int_{s}^{L} T_{\text{base,i}} \frac{d\vec{t}_{ci}(\xi)}{d\xi} \times (\vec{u}(s) - \vec{u}_{ci}(\xi))\, d\xi - \big(T_{\text{base,i}}\vec{t}_{ci}(L)\big) \times (\vec{u}(s) - \vec{u}_{ci}(L))] \tag{15}$$

By taking the derivative of (15) with respect to arc length s, we can obtain the following first-order ordinary differential equation describing the shape of VC-CM based on its neutral axis curvature:

$$E\kappa(s)J'(s) + EJ(s)\kappa'(s) = \sum_{i=1}^{2}[-T_{\text{base,i}} \frac{d\vec{t}_{ci}(s)}{ds} \times (\vec{u}(s) - \vec{u}_{ci}(s)) - \big(T_{\text{base,i}}\vec{t}_{ci}(s)\big) \times \vec{t}(s)] \tag{16}$$

For a conical-shaped VC-CM using two actuation tendons T_{base1} and T_{base2}, shown in Fig. 2, equation (16) can be simplified to the following algebraic form [10]:

$$\kappa'(s) = -\frac{E\kappa(s)J'(s)}{\sum_{i=1}^{2} d_{ci}^2 T_{\text{base,i}} + EJ(s)} \tag{17}$$

To solve (17), the initial value of curvature can be obtained from the boundary condition at the tip position (i.e., $s = L$). Equations (1) and (17) then form a system of ordinary differential equations that can be simultaneously solved to obtain the neutral axis curvature and shape of the VC-CM represented by local 2D Frenet–Serret reference frames $(\vec{t}(s), \vec{n}(s))$ [10]. Of note, using (3), the tendon(s) curvature can be easily calculated from the obtained $\kappa(s)$ to shift the curvature of the midline to that of tendon(s) $\kappa_{ci}(s)$.

2) Step 2: Iterative Algorithm for Solving (14) when $F_{CDDF} \neq 0$: In this step, we use the obtained curvature and shape in Step 1 (i.e., the friction-less model) as the initial guess to iteratively solve (14). The resulted new VC-CM shape and curvature, after solving the nonlinear equation (14), are then used again as the next initial guess for solving the same equation. We repeat this process until the following stopping criterion is satisfied defining the VC-CM tip e_{tip} error:

$$e_{\text{tip}}(j) = \|\vec{u}_{\text{tip}}(j+1) - \vec{u}_{\text{tip}}(j)\|_2 \leq e_{\text{tip,th}} \tag{18}$$

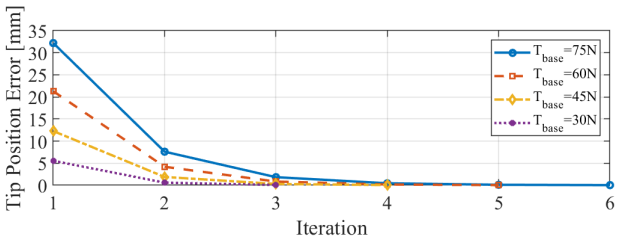

Fig. 3. Convergence of the algorithm based on the tip position error.

where $\vec{u}_{\text{tip}}(j^{\text{th}})$ represents the tip position of the VC-CM at the j^{th} iteration and $e_{\text{tip,th}}$ is the considered stopping threshold for the calculated VC-CM tip error.

Using the proposed algorithm, obviously, the maximum curvature $\kappa_{\text{max}}(s)$ is always obtained from the first step corresponding to the friction-less model with zero loss in the tendon(s) tension. On the other hand, the next iteration, using Step 2 and with initial curvature $\kappa_{\text{max}}(s)$, always yields the minimum curvature $\kappa_{\text{min}}(s)$ with the maximum friction loss for the VC-CM tendon(s) (check equation (10)). Therefore, based on the derived equations and the *squeeze (or sandwich)* theorem, the final obtained shape/curvature $\kappa_{\text{final}}(s)$ using the proposed algorithm always converges to its final shape after a few iterations.

IV. Performance Evaluations

To evaluate the performance of the derived analytical approach and its proposed iterative solution described in Sections II-D and III, we have performed studies in simulations and experiments. The following sections describe these studies in details:

A. Simulation Studies

For our simulations performed in MATLAB (MathWorks, Inc.), we considered a conical-shaped VC-CM with the following parameters defined in Fig. 2: $L = 140$ mm, $d_{ci} = a_i = b_i = 10$ mm, $R_{\text{outer,0}} = 20$ mm, $r_{\text{outer,0}} = 13$ mm, $R_{\text{inner,0}} = r_{\text{inner,0}} = 7$ mm, $E = 1.4$ MPa, and $\mu = 0.42$. Of note, Young's modulus and the friction coefficient were selected based on a silicone (Smooth-Sil 940, Smooth-On, Inc.) used for molding a VC-CM for our experiments and described in Section IV-B.

To evaluate the performance of the model and the proposed iterative solution, we applied different tensions on one tendon at the VC-CM base and evaluated the convergence behavior of the proposed algorithm. Of note, for these simulations, we considered $e_{\text{tip,th}} = 0.1$ mm as the stopping criterion for our algorithm. Fig. 3 demonstrates the results of this study. Also, Fig. 4 shows the calculated shapes of the VC-CM (i.e., its midline) at each iteration for the case of $T_{\text{base}} = 75N$. Fig. 5 indicates the calculated distributed cable tension $T_{\text{tendon}}(s)$, normal force $F_{\text{CDDN}}(s)$, and friction force $F_{\text{CDDF}}(s)$ along the tendon arc length for the case of $T_{\text{base}} = 75$ N. In addition, Fig. 6 compares the calculated VC-CM shapes, midlines, and tendon arc lengths for the cases of $T_{\text{base}} = 10$ N and $T_{\text{base}} = 75$ N. It also shows the calculated $F_{\text{CDDN}}(s)$ and $F_{\text{CDDF}}(s)$ force vectors (i.e., directions, and scaled magnitudes) along the tendon arc length.

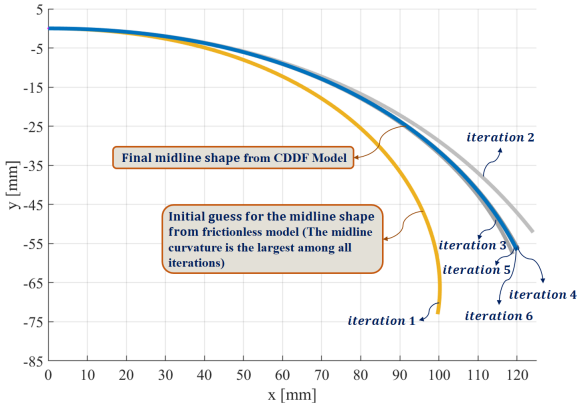

Fig. 4. Estimated midline shapes at each iteration for $T_{base} = 75$ N.

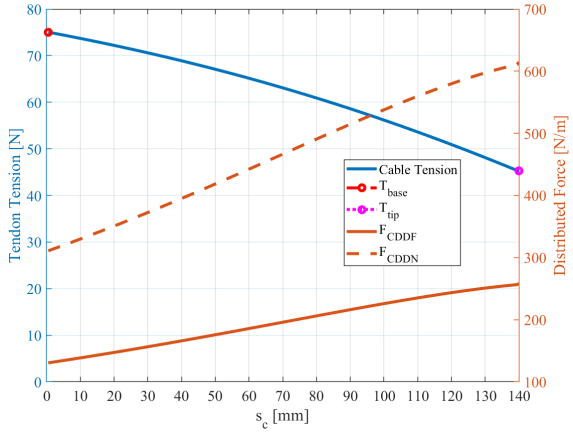

Fig. 5. Calculated distributed forces ($T_{\text{tendon}}(s)$, $T_{\text{CDDN}}(s)$ and $T_{\text{CDDF}}(s)$) along the VC-CM tendon arc length for $T_{base} = 75$ N.

B. Experimental Studies

Fig. 7 shows the experimental setups fabricated for evaluating the performance of the derived equations and the iterative algorithm. For these experiments, we used a silicone (Smooth-Sil 940, Smooth-On, Inc.) with Young's modulus of $E = 1.4$ MPa to mold a VC-CM (shown in Fig. 7b) with the dimensions described in Section IV-A. As shown in Fig. 7a, we also used this silicone to mold a sheath (outer diameter = 7 mm and inner diameter = 2 mm) to measure the friction coefficient between the sheath and the actuation wire rope (34235T28, McMaster-Carr) with outer diameter of 0.046 inch. To measure this friction coefficient, we first mounted the molded sheath around a 3D printed pulley with radius of 3 inch (Fig. 7a), passed the wire rope through the sheath, and then fixed one end of the wire to a load cell (LSB201, FUTEK Advanced Sensor Technology, Inc.) and its other end to various lab weights. Given known tensions on two sides of the wire rope and using (5), we obtained friction coefficient $\mu = 0.42$.

Since Distributed Friction Force and Shape/Curvature in a TD-CM are interrelated, we only evaluated the proposed model by measuring the tendon-tension transmission loss. To this end, we used the setup shown in Fig. 7b to evaluate the performance of the presented model and its solution algorithm in obtaining the tendon's tension at the VC-CM tip T_{tip} for various base tensions. To measure T_{base}, we

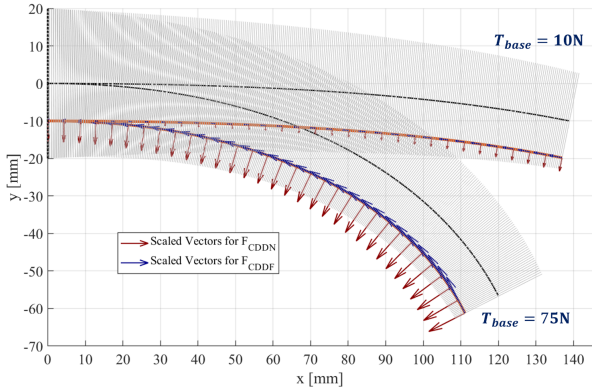

Fig. 6. Calculated $F_{\text{CDDN}}(s)$ and $F_{\text{CDDF}}(s)$ force vectors (i.e., directions, and scaled magnitudes) along the tendon arc length.

used a tension load cell (LSB201, FUTEK Advanced Sensor Technology, Inc.) while for T_{tip}, we utilized a through hole compression load cell (LTH300, FUTEK Advanced Sensor Technology, Inc.). To generate various T_{base} and a continuous bending motion for the VC-CM, we used a micro meter head (BM25.40, Newport Corporation) and linear stage (M-UMR12.40, Newport Corporation) mechanism to continuously pull the actuation wire rope (Fig. 7b) from the VC-CM initial straight configuration. Fig. 8 reports the results of six repeated experiments in which 18 tensions at the base ($T_{base} = 5$ N- 85N with 5N increments) and tip of the VC-CM using the described load cells were measured. This figure also compares these measurements with the obtained results from the model and iterative solution.

V. Discussion

The simulation results shown in Fig. 3 and Fig. 4 demonstrate the successful performance of the proposed iterative algorithm in fast convergence to the final VC-CM shape for different tendon tensions. As discussed in Section III-.2 and can be observed in Fig. 4, the initial shape obtained based on the friction-less model (i.e., equation (17)) resulted in the maximum curvature, while the first iteration based on this initial curvature resulted in the minimum curvature for the VC-CM because of the maximum tension loss due to the friction. Additionally, based on the squeeze theorem, the final converged shape is located between these two curvatures. Fig. 3 also indicates the efficacy of the proposed algorithm by dramatically reducing the VC-CM tip position after the first iteration. As can be observed in this figure, for the maximum base tendon tension (i.e., $T_{base} = 75$ N), the algorithm errors are less than the considered thresholds after 6 iterations. Fig. 5 and Fig. 6 clearly demonstrate the importance and effect of the distributed friction force on the deformation behavior of the VC-CM and tendons' tension-loss, which has been ignored in various studies (e.g., [14], [10]). For instance, for the simulated case shown in Fig. 5, about 40% tension loss is observed due to the tendon-sheath friction. These figures also show the relation between the curvature and friction/normal force where higher curvatures, at the tip of the VC-CM, produce a higher friction/normal forces and vice versa.

Comparison between the measured experimental tensions

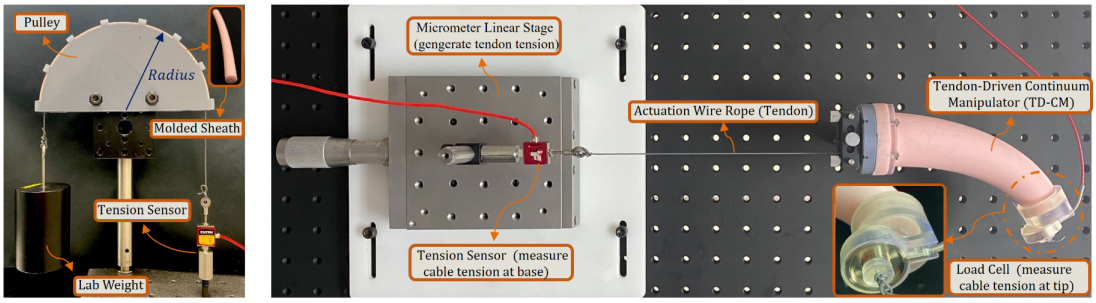

(a) (b)

Fig. 7. (a) Friction coefficient measuring setup; (b) Experimental setup for evaluation of the derived analytical approach and the iterative solution algorithm.

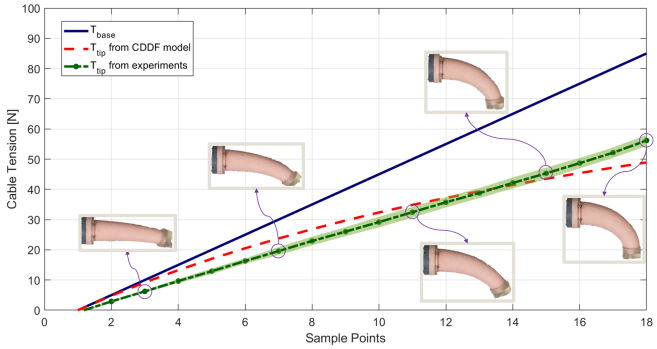

Fig. 8. Comparison of the predicted tensions at the tip of the VC-CM obtained by our analytical model with the measured load cell values. The green shaded region around the experimental results demonstrates the deviation of the six trials from the calculated average.

at the tip of the VC-CM and the tensions obtained using the derived analytical model (shown in Fig. 8) demonstrates the outstanding performance of the derived model (average error of 14.66% between the predicted and measured tensions in 6 repeated experiments) in calculating the tension loss due to the distributed friction force. It is worth re-emphasizing the derived model, despite most of the reported studies in the literature, does not rely on *a priori* knowledge on the shape/curvature of the VC-CM; it instead uses the proposed iterative algorithm in Section III-.2. Of note, the discrepancy between the predicted and experimental results can be partly due to the usage of inaccurate Young's modulus and/or friction coefficient.

VI. Conclusion and Future Studies

In this paper, we presented a novel and analytical approach for modeling curvature-dependent distributed friction force that solves the important problem of tendon-tension transmission losses with a unknown deformation behavior of a generic VC-CM. We showed that the proposed modeling approach does not require a priori knowledge of the VC-CM deformation behavior and can be implemented on a generic VC-CM with a continuous neutral axis function. Our simulation and experimental studies proved the efficacy of the proposed modeling and iterative solution in predicting the VC-CM tendon tension. Our future studies include the extension and experimental evaluation of the current developed model for predicting the deformation behavior and internal forces of a generic VC-CM with 3D bending behavior in the presence of hysteresis and cable slack [15].

References

[1] N. Simaan, R. M. Yasin, and L. Wang, "Medical technologies and challenges of robot-assisted minimally invasive intervention and diagnostics," *Annual Review of Control, Robotics, and Autonomous Systems*, vol. 1, pp. 465–490, 2018.

[2] F. Alambeigi, M. Bakhtiarinejad, S. Sefati, R. Hegeman, I. Iordachita, H. Khanuja, and M. Armand, "On the use of a continuum manipulator and a bendable medical screw for minimally invasive interventions in orthopedic surgery," *IEEE Transactions on Medical Robotics and Bionics*, vol. 1, no. 1, pp. 14–21, 2019.

[3] F. Alambeigi, Y. Wang, S. Sefati, C. Gao, R. J. Murphy, I. Iordachita, R. H. Taylor, H. Khanuja, and M. Armand, "A curved-drilling approach in core decompression of the femoral head osteonecrosis using a continuum manipulator," *IEEE Robotics and Automation Letters*, vol. 2, no. 3, pp. 1480–1487, 2017.

[4] H. Choi, H.-S. Kwak, Y.-A. Lim, and H.-J. Kim, "Surgical robot for single-incision laparoscopic surgery," *IEEE Transactions on Biomedical Engineering*, vol. 61, no. 9, pp. 2458–2466, 2014.

[5] V. Agrawal, W. J. Peine, and B. Yao, "Modeling of transmission characteristics across a cable-conduit system," *IEEE Transactions on Robotics*, vol. 26, no. 5, pp. 914–924, 2010.

[6] R. Roy, L. Wang, and N. Simaan, "Modeling and estimation of friction, extension, and coupling effects in multisegment continuum robots," *IEEE/ASME Transactions on Mechatronics*, vol. 22, no. 2, pp. 909–920, 2016.

[7] B. A. Jones and I. D. Walker, "Kinematics for multisection continuum robots," *IEEE Transactions on Robotics*, vol. 22, no. 1, pp. 43–55, 2006.

[8] R. J. Webster III and B. A. Jones, "Design and kinematic modeling of constant curvature continuum robots: A review," *The International Journal of Robotics Research*, vol. 29, no. 13, pp. 1661–1683, 2010.

[9] J. Till, V. Aloi, and C. Rucker, "Real-time dynamics of soft and continuum robots based on cosserat rod models," *The International Journal of Robotics Research*, vol. 38, no. 6, pp. 723–746, 2019.

[10] F. Renda, M. Cianchetti, M. Giorelli, A. Arienti, and C. Laschi, "A 3d steady-state model of a tendon-driven continuum soft manipulator inspired by the octopus arm," *Bioinspiration & biomimetics*, vol. 7, no. 2, p. 025006, 2012.

[11] A. Gao, R. J. Murphy, H. Liu, I. I. Iordachita, and M. Armand, "Mechanical model of dexterous continuum manipulators with compliant joints and tendon/external force interactions," *IEEE/ASME Transactions on Mechatronics*, vol. 22, no. 1, pp. 465–475, 2016.

[12] J. Jung, R. S. Penning, N. J. Ferrier, and M. R. Zinn, "A modeling approach for continuum robotic manipulators: Effects of nonlinear internal device friction," in *2011 IEEE/RSJ International Conference on Intelligent Robots and Systems*, pp. 5139–5146, IEEE, 2011.

[13] G. Subramani and M. R. Zinn, "Tackling friction-an analytical modeling approach to understanding friction in single tendon driven continuum manipulators," in *2015 IEEE International Conference on Robotics and Automation (ICRA)*, pp. 610–617, IEEE, 2015.

[14] D. C. Rucker and R. J. Webster III, "Statics and dynamics of continuum robots with general tendon routing and external loading," *IEEE Transactions on Robotics*, vol. 27, no. 6, pp. 1033–1044, 2011.

[15] P. Esmatloo and A. D. Deshpande, "Fingertip position and force control for dexterous manipulation through model-based control of hand-exoskeleton-environment," in *2020 IEEE International Conference on Advanced Intelligent Mechatronics (AIM)*, IEEE, 2020.